ADVANCED FUNCTIONAL MATERIALS

Supporting Information

for *Adv. Funct. Mater.*, DOI 10.1002/adfm.202306742

Designing Reflective Hybrid Counter Electrode for Fiber Dye-Sensitized Solar Cell with Record Efficiency

*Zhengfeng Zhu, Zhengmeng Lin, Yu Gu, Jiatian Song, Xinyue Kang, Hongyu Jiang and Huisheng Peng**

Supporting Information for

Designing Reflective Hybrid Counter Electrode for Fiber Dye-Sensitized Solar Cell with Record Efficiency

*Zhengfeng Zhu[1†], Zhengmeng Lin[1†], Yu Gu[2†], Jiatian Song[1], Xinyue Kang[1], Hongyu Jiang[1], and Huisheng Peng[1]**

[1]State Key Laboratory of Molecular Engineering of Polymers, Department of Macromolecular Science and Laboratory of Advanced Materials, Fudan University, Shanghai 200438, China.

[2]Key Laboratory of Advanced Display Materials and Devices, Ministry of Industry and Information Technology, Institute of Optoelectronics & Nanomaterials, College of Material Science and Engineering Nanjing University of Science and Technology, Nanjing, 210094, China

[†]These authors contributed equally to this work.

Corresponding Email: penghs@fudan.edu.cn

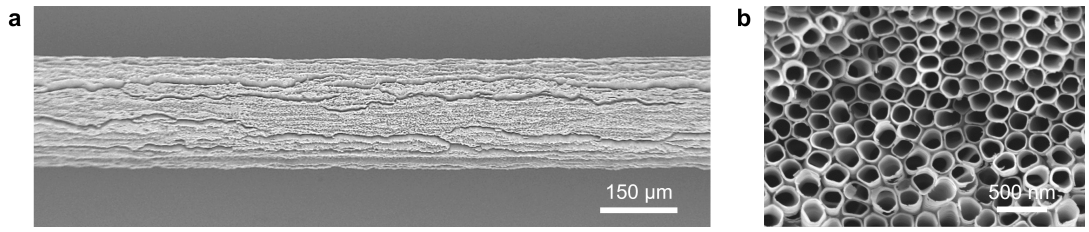

Figure S1. (**a**) SEM image of fiber photoanode. (**b**) High-resolution SEM image of the fiber photoanode with TiO_2 nanotube array.

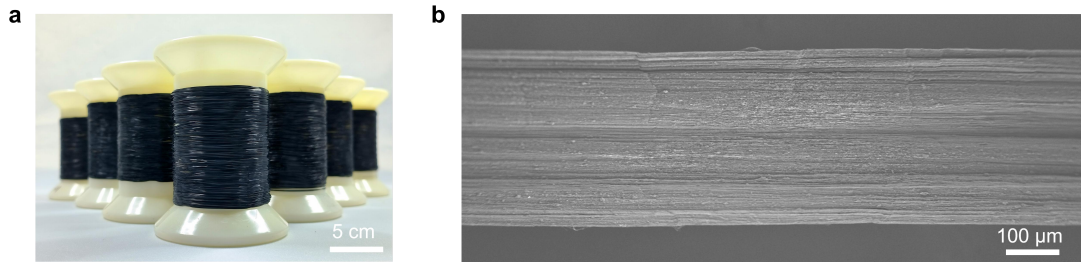

Figure S2. (**a**) Photograph of CNT sheets winded on several reels. (**b**) SEM image of the aligned CNT sheet.

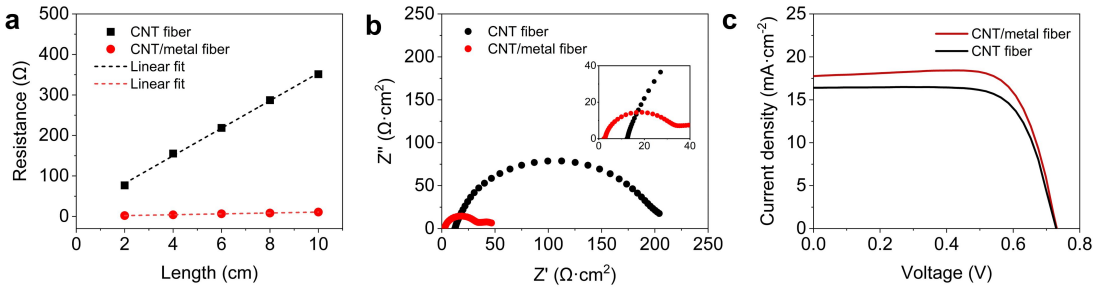

Figure S3. (**a**) Electrical resistances of CNT fibers with and without metal current collector, which were 1.081 and 34.77 Ω·cm^{-1}, respectively. (**b**) Nyquist plots of symmetrical cells fabricated with two identical electrodes measured at 0 V from 100 kHz to 0.01 Hz in the 3-methoxypropionitrile solution containing 6 mM I_2, 0.1 M LiI, 0.6 M 1,2-dimethyl-3-propylimidazolium iodide, and 1 M 4-tert-butylpyridine. Inset, enlarged view of Nyquist plots at high frequency. The corresponding series resistance (R_S), charge transfer resistances (R_{CT}), and Nernst diffusion resistance (Z_N) of twisted CNT fibers were 12.43, 0.94 and 186.52 Ω·cm^2, respectively, while the R_S, R_{CT}, and Z_N of CNT/metal fiber were 2.24, 0.52, and 31.10 Ω·cm^2, respectively. (**c**) *J-V* curves of FDSSCs with twisted CNT fiber and CNT/metal fiber. The PCE of FDSSC using twisted CNT fiber was 8.61% with a J_{SC} of 16.406 mA·cm^{-2}, a V_{OC} of 0.732 V, and an *FF* of 0.716. Due to more efficient charge collection and transport for lower charge recombination, the FDSSC using CNT/metal fiber achieved higher J_{SC} and *FF,* producing a higher PCE of 9.74% with a J_{SC} of 17.782 mA·cm^{-2}, a V_{OC} of 0.733 V, and an *FF* of 0.747.

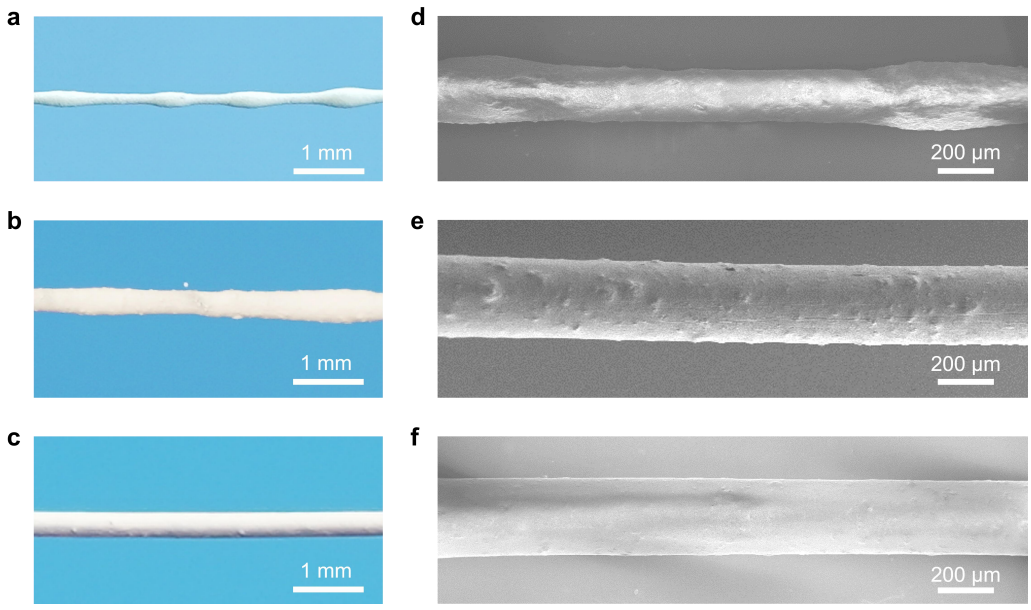

Figure S4. (**a**–**c**) Photographs of CNT/metal fibers after dip-coating with the as-prepared TiO_2/P(VDF-HFP) slurries with TiO_2 contents of 5.56 wt% (**a**), 12.82 wt% (**b**), and 24.44 wt% (**c**), corresponding to slurry viscosities of 2.91, 5.32, and 19.96 Pa·s, respectively. (**d**–**f**) Corresponding SEM images in (**a**–**c**). The slurry with low viscosity produced obvious agglomeration such as beads on the fiber. The increasing concentration of TiO_2 effectively enhanced the viscosity of the slurry to overcome its surface tension, beneficial for the formation of a uniform film on CNT/metal fiber.

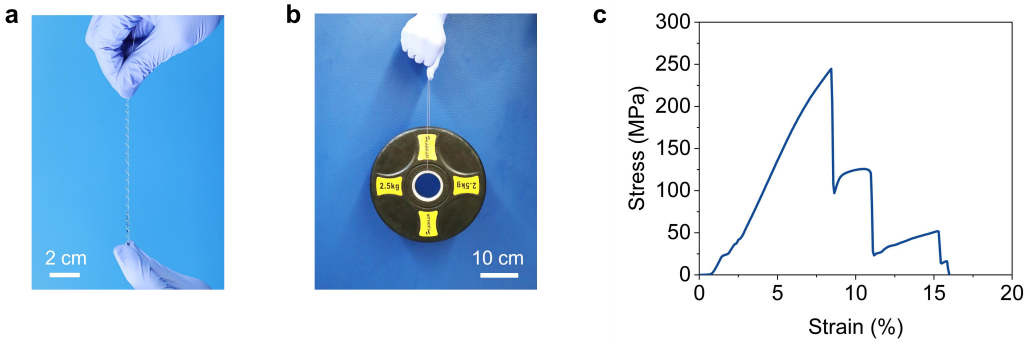

Figure S5. (a) Photograph of the hybrid counter electrode winding around a rod with radius of 1 mm. (b) Photograph of the hybrid counter electrode hanging a barbell sheet with weight of 2.5 kg. (c) Stress-strain curve of the hybrid counter electrode. The resulting hybrid counter electrode could suffer tensile stress within 244.6 MPa without breakage, fully meeting the demands of weaving applications.

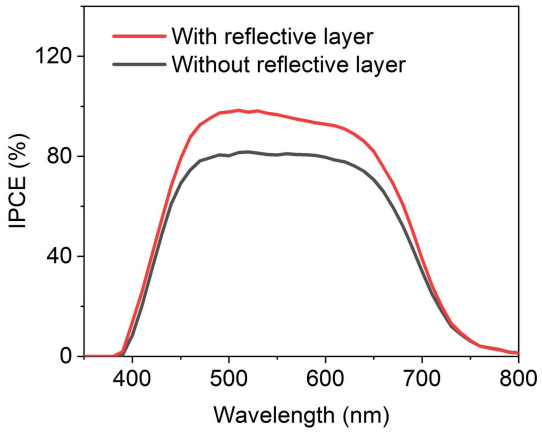

Figure S6. IPCE spectra of FDSSCs with and without reflective layer, showing the highest IPCE values of 98.35% and 81.76% at 520 nm, respectively. The FDSSC with reflective layer exhibited a marked increase in the photogenerated electrons, demonstrating efficiently enhanced light harvesting.

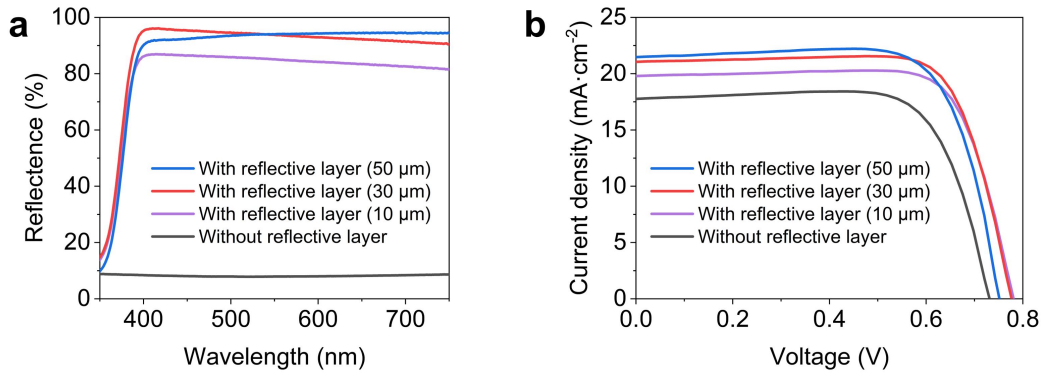

Figure S7. (**a**) Reflectance spectra curves of CNT sheets without reflective layer and coated with reflective layers including different thicknesses of 10, 30, and 50 μm. (**b**) Corresponding *J-V* curves of FDSSCs without reflective layer and with reflective layers including different thicknesses of 10, 30, and 50 μm.

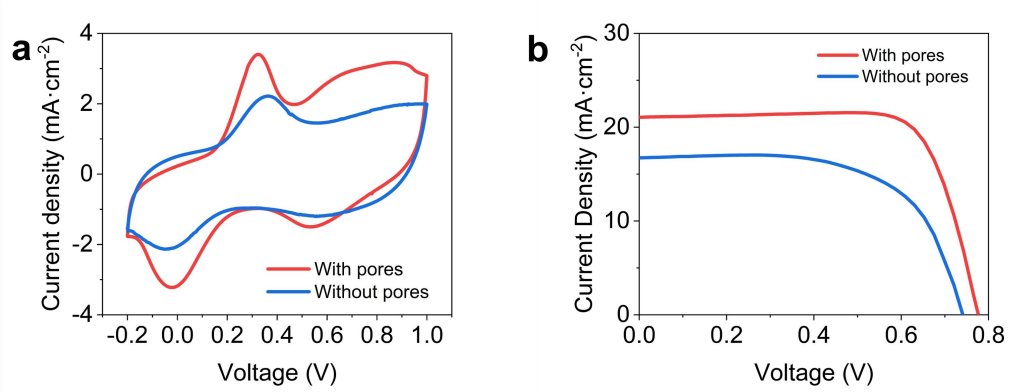

Figure S8. (**a**) Cyclic voltammograms of the hybrid electrodes with and without pores were measured in a three-electrode system using Pt as the counter electrode, Ag/AgCl as the reference electrode, and the acetonitrile solution containing 5 mM I^-, 0.5 mM I_2, and 0.05 M $LiClO_4$ as electrolyte. The scan rate was 50 $mV \cdot s^{-1}$. The diameters of both the hybrid electrodes with and without pores were ~252 μm. As the high peak current density in CV curves generally showed the counter electrode owned enhanced electrocatalytic activity to generate higher photocurrent, the hybrid electrode with pores showed higher electrocatalytic activity for I^-/I_3^- redox couples than that without pores reflected more electrochemical active areas. (**b**) *J-V* curves of FDSSCs using reflective layers with and without pores. The PCE of FDSSC using reflective layers with pores was as high as 12.52%, with a J_{SC} of 21.061 $mA \cdot cm^{-2}$, a V_{OC} of 0.777 V, and an *FF* of 0.765. In contrast, the FDSSC using reflective layers without pores showed a much lower PCE of 7.92%, with a J_{SC} of 16.736 $mA \cdot cm^{-2}$, a V_{OC} of 0.739 V, and an *FF* of 0.640. The much higher impendence and much lower electrocatalytic activity of the counter electrode with a dense reflective layer caused severe charge recombination and seriously decreased J_{SC} and *FF*.

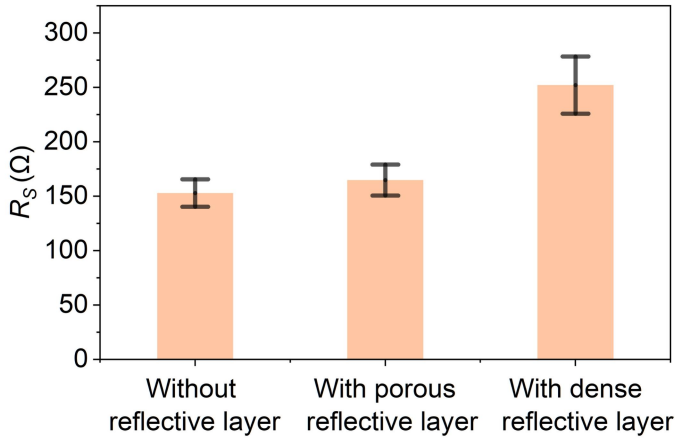

Figure S9. (a) R_S values of FDSSCs with different counter electrodes. Error bars, standard deviations of the results from ten samples. The R_S in FDSSCs using the counter electrode with dense reflective layer was greatly increased, while the FDSSCs with porous reflective layer only showed slightly higher R_S values than those without reflective layer, which also accounted for their high PCEs.

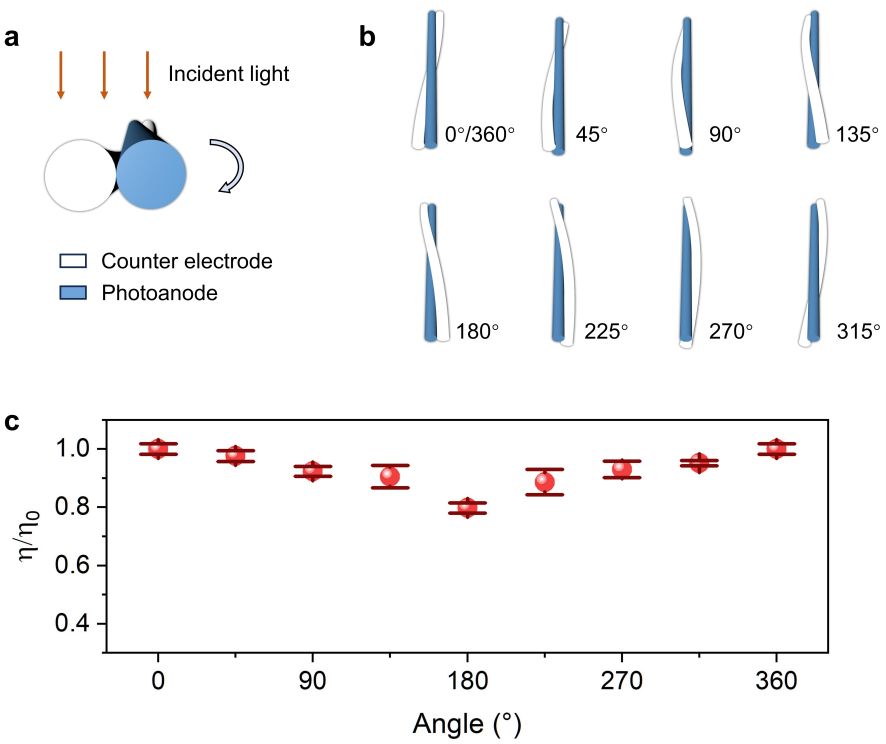

Figure S10. (a) Schematic diagram of the FDSSC under the incident light. (b) Schematics illustrating the top views of FDSSCs placed with different angles under the incident light to explore their PCE dependency on the incident light direction. (c) Corresponding photovoltaic performances of FDSSCs placed with different angles. The PCEs of FDSSCs had been maintained by over 90% under the incident light from different directions at a broad range. The largest PCE variation of ~20% emerged with FDSSCs placed at 180°, as the counter electrode partly covered on the photoanode had the most influence on light harvesting under this condition.

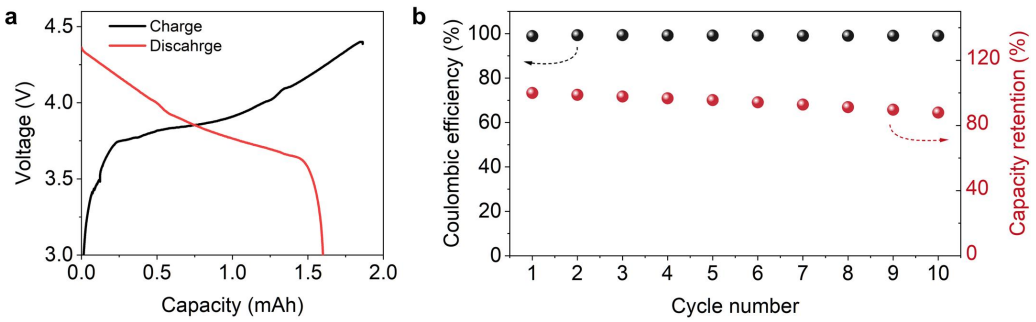

Figure S11. (a) Typical charge and discharge profiles of a fiber lithium-ion battery. The fiber lithium-ion battery was first charged from 3 to 3.5 V at 0.02 C rate and from 3.5 to 4.4 V at 0.2 C rate, then charged under 4.4 V until the current was below 0.05 C, and subsequently discharged to 3 V at 0.2 C rate, showing a capacity of 1.6 mAh. (b) Corresponding cycling performance and coulombic efficiency of fiber lithium-ion battery after photocharging/discharging for 10 cycles. The fiber lithium-ion battery was charged by FDSSCs with a current of 1.5 mA, and then discharged to 2.8 V at 0.5C rate.

Table S1. Photovoltaic parameters of the FDSSCs in Figure S7b.

	V_{oc}/(V)	J_{sc}/(mA·cm^{-2})	FF	PCE (%)
Without reflective layer	0.733	17.782	0.747	9.74
With reflective layer (10 μm)	0.781	19.816	0.768	11.90
With reflective layer (30 μm)	0.777	21.061	0.765	12.52
With reflective layer (50 μm)	0.751	21.51	0.756	12.23

Table S2. EIS data in Figure 3e.

	R_s/(Ω·cm^2)	R_{ct}/(Ω·cm^2)	Z_N/(Ω·cm^2)
Without reflective layer	2.24	0.52	31.10
With porous reflective layer	3.45	0.34	34.22
With dense reflective layer	7.67	0.98	73.24

Table S3. Structure and photovoltaic parameters of typical FDSSCs.

Device structure	V_{OC} (V)	J_{SC} (mA/cm^2)	*FF*	PCE (%)	Ref.
Ti wire/TiO_2 nanoparticle layer/N719/ I^--I_3^-/Pt wire	0.68	10.60	0.83	6.00	[1]
Ti wire/TiO_2 nanotube array/N719/ I^--I_3^-/CNT@Graphene fiber	0.69	13.55	0.73	6.83	[2]
Ti wire/TiO_2 nanotube array/N719/ I^--I_3^-/$CoNi_2S_4$ nanoribbon-CF	0.68	15.30	0.68	7.03	[3]
Ti wire/TiO_2 nanotube array/N719/ I^--I_3^-/MWCNT array	0.71	16.00	0.61	7.13	[4]
Ti wire with microridges: nano rods/ TiO_2 NPs/N719/ I^--I_3^-/Pt wire	0.70	14.79	0.78	8.13	[5]
Ti wire/TiO_2 nanotube array/N719/ I^--I_3^-/Graphene fiber	0.73	17.11	0.67	8.41	[6]
Ti wire/TiO_2 nanotube array/N719/ I^--I_3^-/Pt:CS-CNT composite fiber	0.73	19.43	0.71	10.00	[7]
Ti wire/TiO_2 nanotube array/N719/ I^--I_3^-/CF@PANI@CoSe composite fiber	0.73	17.65	0.80	10.28	[8]
Ti wire/TiO_2 nanotube array/PEOx/N719/ I^--I_3^-/Pt wire	0.81	17.10	0.81	11.22	[9]
Ti wire TiO_2 nanotube array/N719/Co^{2+}-Co^{3+}/Hierarchically assembled CNT@Pt composite fiber	0.91	19.32	0.68	11.94	[10]
Ti wire/TiO_2 nanotube array/N719/ I^--I_3^-/metal@CNT fiber	0.73	17.78	0.75	9.74	This work
Ti wire/TiO_2 nanotube array/N719/ I^--I_3^-/metal@CNT with reflective fiber	0.78	21.06	0.77	12.52	This work

References

[1] X. Pu, W. Song, M. Liu, C. Sun, C. Du, C. Jiang, X. Huang, D. Zou, W. Hu, Z. L. Wang, *Adv. Energy Mater.* **2016**, 6, 1601048.

[2] X. Fang, Z. Yang, L. Qiu, H. Sun, S. Pan, J. Deng, Y. Luo, H. Peng, *Adv. Mater.* **2014**, 26, 1694.

[3] L. Chen, Y. Zhou, H. Dai, T. Yu, J. Liu, Z. Zou, *Nano Energy* **2015**, 11, 697.

[4] Z. Yang, J. Deng, X. Sun, H. Li, H. Peng, *Adv. Mater.* **2014**, 26, 2643.

[5] G. Liu, M. Wang, H. Wang, R. E. A. Ardhi, H. Yu, D. Zou, J. K. Lee, *Nano Energy* **2018**, 49, 95.

[6] Z. Yang, H. Sun, T. Chen, L. Qiu, Y. Luo, H. Peng, *Angew. Chem. Int. Ed.* **2013**, 52, 7545.

[7] X. Fu, H. Sun, S. Xie, J. Zhang, Z. Pan, M. Liao, L. Xu, Z. Li, B. Wang, X. Sun, H. Peng, *J. Mater. Chem. A* **2018**, 6, 45.

[8] J. Zhang, Z. Wang, X. Li, J. Yang, C. Song, Y. Li, J. Cheng, Q. Guan, B. Wang, *ACS Appl. Energy Mater.* **2019**, 2, 2870.

[9] R. E. A. Ardhi, M. X. Tran, M. Wang, G. Liu, J. K. Lee, *J. Mater. Chem. A* **2020**, 8, 2549.

[10] X. Kang, Z. Zhu, T. Zhao, W. Zhai, J. Xu, Z. Lin, K. Zeng, B. Wang, X. Sun, P. Chen, H. Peng, *Adv. Funct. Mater.* **2022**, 32, 2207763.